

# Hall drift of fractional Chern insulators in few-boson systems

C. Repellin,<sup>1,\*</sup> J. Léonard,<sup>2</sup> and N. Goldman<sup>3,†</sup>

<sup>1</sup>Univ. Grenoble-Alpes, CNRS, LPMMC, 38000 Grenoble, France

<sup>2</sup>Department of Physics, Harvard University, Cambridge, Massachusetts 02138, USA

<sup>3</sup>CENOLI, Université Libre de Bruxelles, CP 231, Campus Plaine, B-1050 Brussels, Belgium

(Dated: July 7, 2022)

Realizing strongly-correlated topological phases of ultracold gases is a central goal for ongoing experiments. And while fractional quantum Hall states could soon be implemented in small atomic ensembles, detecting their signatures in few-particle settings remains a fundamental challenge. In this work, we numerically analyze the center-of-mass Hall drift of a small ensemble of hardcore bosons, initially prepared in the ground state of the Harper-Hofstadter-Hubbard model. By extracting the Hall conductivity in a wide range of the magnetic flux, we identify an emergent Hall plateau compatible with a fractional Chern insulator state: the width of the plateau agrees with the spectral and topological properties of the prepared ground state, while the Hall conductivity approaches a fractional value determined by the many-body Chern number. A comparison with a direct application of Streda's formula is also discussed. Our calculations suggest that fractional Chern insulators can be detected in cold-atom experiments, using available detection methods.

*Introduction.* Important progress is being made in view of realizing strongly-correlated topological phases of ultracold atoms in optical lattices [1, 2]. On the one hand, experimental efforts have been dedicated to the creation of artificial gauge fields [3, 4] and topological bands [2] for neutral atoms, leading to measurements of topological properties [5–21]. On the other hand, theoretical studies have identified realistic schemes for preparing small atomic ensembles in fractional Chern insulators (FCIs) [22–29], which are lattice analogues of fractional quantum Hall (FQH) liquids [30, 31]; they also proposed methods to probe their characteristic features [32–42]. This progress should soon lead to the realization of FCIs in small atomic ensembles, and to the possibility of observing their properties. However, identifying clear and accessible topological signatures of FCIs in small interacting atomic systems still constitutes a central challenge. In fact, this question concerns a wide range of quantum-engineered platforms, including strongly-interacting photonic systems [43–45].

The canonical signature of FQH states is provided by the Hall conductivity, i.e. the linear-response coefficient relating an induced transverse current to the applied force. In the FQH effect, the Hall conductivity is quantized to a value  $\sigma_H/\sigma_0 \in \mathbb{Q}$  in the thermodynamic limit [46];  $\sigma_0^{-1} = R_K$  is von Klitzing's constant. The Hall response is also accessible in ultracold atoms; it has been measured in weakly-interacting gases through various probes, including center-of-mass (COM) drifts [6, 17, 21, 47–49] and local currents [20, 50], and more indirectly, through collective-mode excitations [51] and circular dichroism [18]. Whether the Hall response could be used to detect FCIs in few-body systems remains an important question to be addressed.

In this Letter, we numerically analyze the Hall drift of a small ensemble of strongly-interacting (hardcore) bosons, initially prepared in the ground state of the Harper-Hofstadter-Hubbard model [52, 53]. Building on Refs. [6, 54], we monitor the COM of the prepared state upon releasing it into a larger lattice while applying a weak static force. This Hall drift measurement, which provides an estimation of the Hall

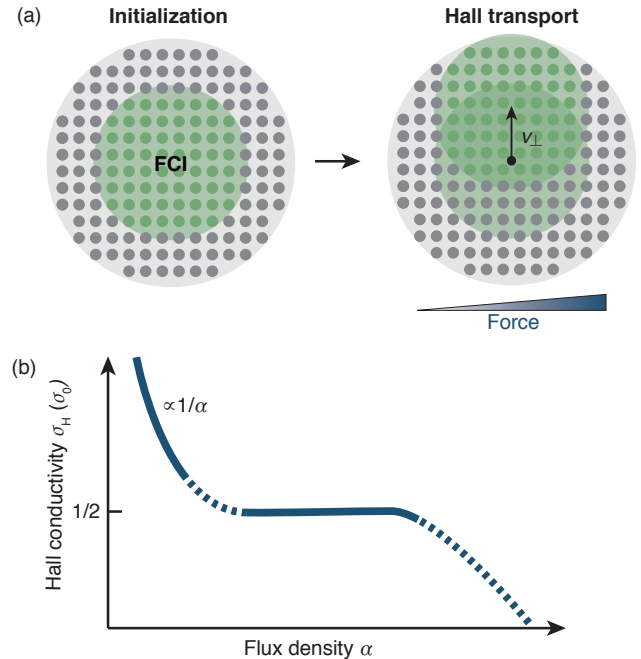


Figure 1. (a) Hall drift protocol: a prepared fractional Chern insulator (FCI) state is released into a larger lattice and a uniform force is applied. The Hall conductivity is extracted from the COM drift transverse to the force. (b) Sketch of the Hall conductivity  $\sigma_H(\alpha)$  as a function of the flux density in the Harper-Hofstadter-Hubbard (HHH) model. In the continuum limit  $\alpha \ll 1$ , the system follows the classical prediction  $\sigma_H \sim 1/\alpha$ . In the vicinity of the filling factor  $\nu = \rho_{\text{bulk}}/\alpha = 1/2$ , where  $\rho_{\text{bulk}}$  is the bulk particle density, an FCI is formed and  $\sigma_H(\alpha)$  depicts a Hall plateau.

conductivity in the prepared state, is performed in a wide range of magnetic flux values [Fig. 1]. From this, we identify an emergent Hall plateau, whose width coincides with the region where we identify an FCI ground state through entanglement spectroscopy. Besides, the value indicated by the Hall plateau,  $\sigma_H/\sigma_0 \approx 0.5$ , is a topological marker of the FCI

phase. Our results indicate that FCI states composed of few bosons ( $N \geq 3$ ) can be identified through Hall drifts under realistic experimental conditions. We also compare this approach with a direct application of Streda's formula [55–58].

*The Hall drift protocol.* We extract the Hall conductivity  $\sigma_H$  from the COM drift of an initially prepared state upon applying a weak external force. This COM probe [6, 54, 59] is particularly suitable when considering a small ensemble of particles, for which local currents substantially fluctuate. In order to limit boundary effects, we release the initially prepared state into a larger lattice [54, 60] before monitoring the COM drift. This protocol is implementable in cold-atom experiments, where tunneling can be dynamically tuned and COM motion measured [6, 17, 21, 47–49]. In our simulations, the time scales associated with the progressive release of the inner system, as well as the duration of the Hall-drift measurement, are adjusted to avoid boundary effects due to the finite simulation box.

The COM Hall drift  $x_\perp(t)$  transverse to the applied force  $F$  allows one to extract the Hall velocity  $v_\perp = x_\perp(t)/t$ , upon reaching a stationary regime within linear response. This Hall velocity is related to the transverse current density through  $v_\perp = j_\perp/\rho_{\text{bulk}}$ , where  $\rho_{\text{bulk}}$  denotes the bulk particle density. From the transport equation,  $j_\perp = \sigma_H F$ , one extracts the Hall conductivity through  $\sigma_H/\sigma_0 = (2\pi\rho_{\text{bulk}}/F)v_\perp$ , where  $\sigma_0 = 1/2\pi$  is the conductivity quantum ( $\hbar=1$ ).

For a translationally-invariant quantum system of  $N$  interacting particles in a uniform magnetic field, the COM dynamics are independent of the interaction strength [58, 61, 62] and the Hall conductivity follows the classical prediction,  $\sigma_H \sim 1/\alpha$ , where  $\alpha$  denotes the number of flux quanta ( $\Phi_0 = 2\pi$ ) per unit area. This classical behavior breaks down upon breaking translational symmetry (e.g. by adding a lattice, disorder or an edge [63]), opening the possibility for quantized Hall plateaus  $\sigma_H/\sigma_0 = \nu_{\text{Ch}}^{\text{MB}} \in \mathbb{Q}$  around filling factors corresponding to incompressible states [46, 62]; the quantity  $\nu_{\text{Ch}}^{\text{MB}}$  denotes the many-body Chern number, a topological invariant associated with the ground-state of the many-body system [64, 65].

*Microscopic model and ground-state properties.* We study the emergence of quantized Hall plateaus in the COM dynamics of strongly-interacting bosons moving on a 2D square lattice in the presence of a uniform magnetic flux. The corresponding Harper-Hofstadter-Hubbard (HHH) Hamiltonian reads [52, 53]

$$\hat{H}_0 = -J \left( \sum_{m,n} \hat{a}_{m,n+1}^\dagger \hat{a}_{m,n} + e^{i2\pi\alpha n} \hat{a}_{m+1,n}^\dagger \hat{a}_{m,n} + \text{h.c.} \right) + (U/2) \sum_m \hat{a}_{m,n}^\dagger \hat{a}_{m,n} (\hat{a}_{m,n}^\dagger \hat{a}_{m,n} - 1), \quad (1)$$

where  $\hat{a}_{m,n}^\dagger$  creates a boson at lattice site  $(m, n)$ ,  $J$  denotes the tunneling amplitude,  $U$  is the on-site (Hubbard) interaction strength [66], and where the Peierls phase factors [52] account for the presence of a flux  $\Phi = 2\pi\alpha$  per plaquette. This model has been implemented in ultracold-atom experiments [67] using Floquet engineering [1, 2].

Numerical simulations using periodic boundary conditions have established that the HHH model hosts a bosonic FCI akin to the Laughlin state [46], for strongly repulsive interactions and filling factor  $\nu = \rho_{\text{bulk}}/\alpha = 1/2$ ; see Refs. [26–28, 32, 53, 68]. For hardcore bosons, these calculations reveal a stable FCI ground state for  $\alpha \leq 0.3$ ; the bulk gap is maximal around  $\alpha \approx 0.2 - 0.25$  [28, 53, 68], and vanishes in the limit  $\alpha \ll 1$ . This FCI phase is characterized by a fractional many-body Chern number,  $\nu_{\text{Ch}}^{\text{MB}} = 1/2$ , which the Hall conductivity approaches in the thermodynamic limit [40].

In our Hall-drift calculations, we consider  $N$  hardcore bosons initially confined in a circular box containing  $N_s$  lattice sites [Fig. 1(a)]. In this geometry with boundaries, we still expect to find the  $\nu = 1/2$  FCI phase in the regime  $\rho_{\text{bulk}}/\alpha \approx 1/2$ . However, we note that the bulk density  $\rho_{\text{bulk}}$ , which differs from the total density  $\rho = N/N_s$ , has a non-trivial dependence on the flux [70]. Hence, we first analyze the ground-state properties of this few-body system in view of determining the values of  $\rho$  and  $\alpha$  that realize a FCI state.

We first gain some intuition from the physics of the FQH effect in the (continuum) disk geometry [69]. For a flux density  $\alpha \leq 0.3$ , the lowest Bloch band of the single-particle Hofstadter spectrum contains a set of roughly  $N_0(\alpha)$  nearly degenerate states, which are connected to the next band by dispersive edge states [70]. These  $N_0(\alpha)$  states are analogous [33, 34] to the orbitals of the lowest Landau level (LLL) in the disk geometry; there, the  $\nu = 1/2$  Laughlin state with  $N$  bosons occupies  $2N - 1$  LLL orbitals. Likewise, we may expect a  $\nu = 1/2$  FCI state when  $N_0(\alpha) \simeq 2N - 1$ .

We use exact diagonalization to verify the existence of the FCI ground state in our model, and specify its phase boundaries based on (i) the low-energy spectrum; (ii) entanglement spectroscopy; (iii) the occupation of single-particle orbitals. For concreteness, we analyse  $N=4$  bosons in  $N_s=60$  sites:

(i) Figure 2(a) shows the low-energy spectrum of this few-body system; there are three avoided crossings between the ground state and the first excited state within the range  $0 \leq \alpha \leq 0.3$ , which we interpret as the finite-size signatures of three phase transitions. We focus on the regime  $0.15 < \alpha < 0.25$ , where the expected FCI bulk gap is the largest [28, 53], and no phase transition is observed. In this regime, the approximate degeneracy of the lowest band,  $N_0(\alpha) \simeq 7$  [70], is compatible with an FCI ground state candidate for  $N=4$ . We note that the nature of the phases at  $\alpha < 0.15$  is likely to be non-universal due to finite-size effects [71].

(ii) In finite geometries with edges, the topological nature of FCIs can be revealed through the degeneracies of their edge spectrum [33, 34]; however, this spectral signature requires a larger number of sites and a smooth confining potential [72]. Instead, we probe the bulk quasihole excitations of the ground state; their degeneracy is a topological fingerprint of the FCI phase, and it can be extracted from the ground state  $|\Psi_{\text{GS}}\rangle$  using the particle entanglement spectrum [73] (PES). The PES is the spectrum of the reduced density matrix obtained by tracing  $|\Psi_{\text{GS}}\rangle \langle \Psi_{\text{GS}}|$  over a bipartition containing  $N_A$  particles, while keeping the geometry of the system intact. The degeneracy of

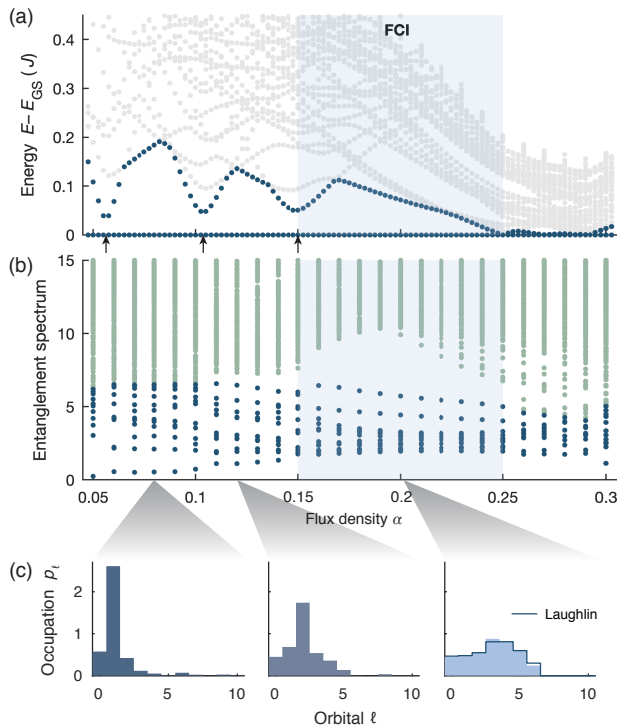


Figure 2. Spectral and topological ground-state properties. We present the ground-state properties for  $N = 4$  hardcore bosons in the HHH model, in a circular box of  $N_s = 60$  sites. The FCI stability region (shaded) is indicated according to three markers: (a) Low-energy many-body spectrum (lowest 10 energies per discrete rotation-symmetry sector) relative to the ground-state energy  $E_{GS}$ . Analyzing absolute energies (not shown) reveals that the three local minima of the gap correspond to level crossings, which are avoided due to finite-size effects (arrows). (b) Particle entanglement spectrum (PES) for a bipartition with 2 particles in each subsystem. In the shaded region, the first 15 levels (blue) are well separated from the other levels, revealing that the ground state is topologically equivalent to the Laughlin state. (c) Occupation of the single-particle orbitals in the ground state (histograms) and in the exact Laughlin state on the disk (line). The orbitals are sorted in increasing energy and angular momentum, respectively.

Laughlin quasiholes is determined through a generalized exclusion principle [74]; for 2 bosons in 7 orbitals, it is 15-fold. And indeed, for  $0.15 < \alpha < 0.25$  and  $N_A = 2$ , the PES in Fig. 2(b) reveals a clear gap above the 15th state, which confirms the FCI nature of  $|\Psi_{GS}\rangle$  in this parameter range.

(iii) To further characterize the ground state, we calculated the occupation of each single-particle orbital. For the Laughlin state on the disk, there is a uniform occupation of all  $2N - 1$  orbitals in the thermodynamic limit, with moderate deviations from this distribution for small systems. We find a similar distribution in the regime  $0.15 \lesssim \alpha \lesssim 0.25$  for the same number of particles [Fig. 2(c)].

Overall, these probes consistently reveal that the ground state is in the  $\nu = 1/2$  FCI phase within the range  $0.15 \lesssim \alpha \lesssim 0.25$ . We have verified that these results are robust with respect to changes in the particle number ( $N = 3, 4$ ) and num-

ber of sites  $N_s$ ; see [70].

*Benchmark using non-interacting fermions.* We first benchmark the Hall-drift measurement by considering non-interacting fermions in the Harper-Hofstadter model, at quarter filling  $\rho = 1/4$ . In this setting, (integer) Chern insulators are expected at flux densities  $\alpha = 1/(4n)$ , with  $n \in \mathbb{Z}$ , where they exhibit quantized Hall plateaus  $\sigma_H/\sigma_0 = n$  in the thermodynamic limit, upon small variations of the flux  $\alpha$ . While this result can be directly deduced from a Diophantine equation [75, 76], the actual size of these plateaus follows a rather complicated law established by the underlying single-particle (Hofstadter-butterfly) spectrum [52]. Furthermore, such Hall plateaus can be altered by finite-size effects. This first numerical study aims to shed some light on these properties.

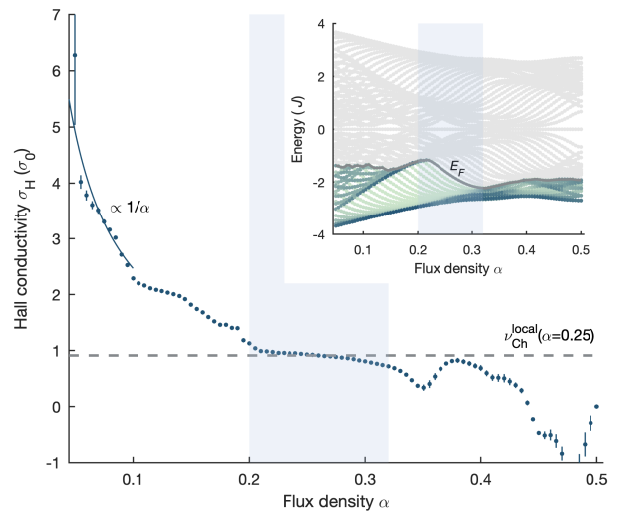


Figure 3. Benchmark using non-interacting fermions. Hall conductivity extracted from the Hall drift of  $N = 20$  fermions, initially prepared in a small circular box of  $N_s = 81$  sites (quarter filling); the release into the larger system (1005 sites) and the ramping up of the force ( $F = 0.2J/d$ ) are performed over a duration  $\tau_{ramp} = 15J^{-1}$ , and the Hall drift measurement over  $\tau_{hold} = 13J^{-1}$ ; the bulk density  $\rho_{bulk}(\alpha)$  is evaluated in a central region of 20 sites;  $\nu_{Ch}^{local}$  denotes the local real-space Chern number; fit error bars reflect the 95% confidence interval. (Inset) Single-particle spectrum  $E(\alpha)$ , for the same box (81 sites); the Fermi level ( $E_F$ ; grey curve) corresponds to the same  $N = 20$ ; filled states are colored in green (bulk states are dark and edge states are light), while empty states are grey;  $E_F$  is located in the main bulk gap (Chern insulator) within the shaded region.

We determine the Hall drift by calculating the time-evolution of  $N = 20$  non-interacting fermions, initially prepared in the ground-state within a circular box of  $N_s = 81$  sites ( $\rho \approx 1/4$ ), which are then released into a larger lattice (1005 sites) and subjected to a weak force  $F = 0.2J/d$ , where  $d$  is the lattice spacing [70]. The Hall conductivity extracted from the stationary (linear-response) Hall drift is depicted as a function of the flux density in Fig. 3. In the low-flux regime ( $\alpha \lesssim 0.1$ ), lattice effects are negligible and the Hall drift follows the classical prediction  $\sigma_H \sim 1/\alpha$ . At  $\alpha = 0.25$ , the Fermi energy lies within the main bulk gap, which yields an approximately quantized value  $\sigma_H/\sigma_0 \approx 0.9$ , dictated by the Chern

number  $\nu_{\text{Ch}} = 1$  of the fully occupied Bloch band [75]; we verified that this measured  $\sigma_{\text{H}}$  matches the value of the local real-space Chern number [77, 78], as averaged over 29 bulk sites in the prepared ground state. The Hall response remains approximately constant for a wide range of flux,  $\alpha \in [0.21, 0.32]$ , in agreement with the Fermi level's location within the main bulk gap of the butterfly spectrum [Fig. 3]; we verified that the flatness of this emergent Hall plateau, as well as the approached quantized value, improve as the system size  $N_s$  increases. These results illustrate how the Hofstadter-butterfly spectrum dictates the size of emergent Hall plateaus in realistic finite-size (non-interacting) settings.

*Hall drift of interacting bosons.* A system of  $N = 4$  bosons is initially prepared in the ground state of the HHH model, using a circular box of  $N_s = 60$  sites. At  $t = 0$ , this bosonic cloud is slowly released into a larger circle (124 sites), while the force is ramped up to the value  $F = 0.01J/d$ ; see [70] for details on the ramps used to reach a stationary regime. Our numerics show that a stationary COM motion takes place after the ramp, over a few tunneling times [inset of Fig. 4], from which we extract the (constant) Hall velocity  $v_{\perp}$ . For longer times, the COM motion is affected by the edge of the finite simulation box, which sets the end of the stationary regime; we point out that this numerical constraint is not an experimental one, since the prepared state can be released into a much larger lattice in realistic setups.

We extract the Hall conductivity  $\sigma_{\text{H}}$ , from the stationary Hall velocity  $v_{\perp}$  and bulk density  $\rho_{\text{bulk}}$ , for a large range of flux values; see Fig. 4. First, we find that the classical behavior  $\sigma_{\text{H}} \sim 1/\alpha$  is recovered [79] in the low-flux (continuum) limit. The correlated behavior of our interacting system then appears for  $\alpha \geq 0.1$ . Most strikingly,  $\sigma_{\text{H}}(\alpha)$  depicts an emergent Hall plateau, whose width matches the flux window associated with the  $\nu = 1/2$  FCI phase [Fig. 2]. In this region, the extracted Hall conductivity approaches the quantized value  $\sigma_{\text{H}}/\sigma_0 \approx 0.5$ , which is expected in the thermodynamic limit. Calculations performed on larger systems (up to  $N = 10$  bosons in  $N_s = 120$  sites) indeed demonstrate convergence to a quantized Hall plateau [70]. Interestingly, a second plateau appears in the range  $\alpha \in [0.1, 0.15]$ , which may signal the onset of the  $\nu = 2/3$  FCI phase [33, 82].

We sought for minimal configurations that exhibit Hall-plateau signatures of the FCI state, by simulating our Hall drift protocol for various system sizes  $N_s$ , considering  $N = 3, 4$  bosons [70]. Our results show that the  $\nu = 1/2$  FCI state can be detected by measuring the COM Hall drift of systems as small as 3 bosons in  $N_s = 40$  sites and 4 bosons in  $N_s = 49$  sites. We note that the evaluation of the bulk density  $\rho_{\text{bulk}}$ , which is used in the Hall-drift measurement of  $\sigma_{\text{H}}$ , is complicated by substantial density fluctuations for such system sizes; nevertheless, we find that the extracted Hall plateaus are robust despite these fluctuations [70].

We finally compared our Hall-drift approach with a direct application of Streda's formula [55–58],  $\sigma_{\text{H}}/\sigma_0 = \partial\rho_{\text{bulk}}/\partial\alpha$ , which relates the quantized Hall conductivity of incompressible states to their bulk density. While we find that Streda's

formula indeed yields a quantized Hall plateau for large systems ( $N = 10$ ,  $N_s = 120$ ), this signature is faint for few-boson settings ( $N = 3, 4$ ); see [70]. The Hall-drift probe thus seems more appropriate to detect FCIs in few-boson systems.

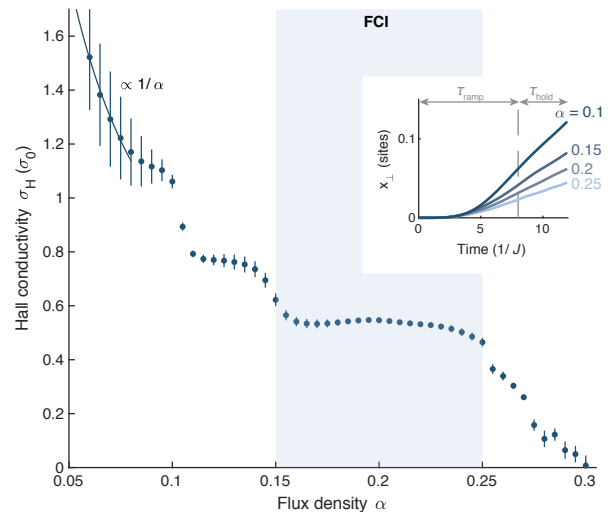


Figure 4. Hall drift of hardcore bosons in the HHH model. After preparation in the ground state, 4 bosons confined in a circular box ( $N_s = 60$ ) are progressively released into a larger box containing 124 sites and subjected to a uniform force  $F = 0.01J/d$ . At the end of this ramp, the COM motion is stationary for a few tunneling times (inset), permitting the extraction of the Hall conductivity; the bulk density  $\rho_{\text{bulk}}(\alpha)$  is evaluated in a central region of 16 sites [70]; fit error bars reflect the 95% confidence interval. The FCI phase (shaded region from Fig. 2) coincides with the emergent Hall plateau.

*Experimental considerations.* For a possible implementation of the proposed protocol, we consider the following experimental scheme. First, the FCI is prepared through adiabatic quantum state engineering, starting from a topologically trivial state and inducing a topological phase transition to an FCI by slowly tuning the Hamiltonian parameters [24–29]. The adiabaticity of this preparation relies on the finite extent of the system, which prevents the many-body gap from vanishing at the transition point. In our scheme, the FCI would be embedded in a lattice with more sites, which are initially uncoupled either by switching off the tunneling to those sites (as assumed in our numerical calculations), or by increasing their energy with a repulsive potential. The drift protocol is initiated by restoring the coupling to outer sites and simultaneously ramping up a force induced by, for instance, an optical or magnetic potential gradient [6, 48]. Finally, the Hall drift is detected by measuring the COM position after variable drift times. Detecting COM displacements smaller than one lattice site, as depicted in Fig. 4, is within the current capabilities of cold-atom experiments [67]. Yet, we expect that even stronger signatures are possible because experiments allow access to total system sizes and drift times beyond the reach of exact numerics. In addition, the ability to choose finite interactions and to tune them dynamically opens up the possibility for advanced transport studies. The simplicity of this realistic exper-

imental scheme paves the way to the exploration of quantum transport in strongly-correlated ultracold topological matter.

During completion of our manuscript, we became aware of a recent work [80], which also analyses the Hall response of an FCI in the HHH model.

*Acknowledgments* We thank M. Greiner for insightful discussions. We acknowledge J. Motruk and I. Na for sharing their manuscript [80] before submission, and for their comments on our work. DMRG calculations were performed using the TeNPy Library (version 0.4.0) [81]. C.R. is supported by the Marie Skłodowska-Curie program under EC Grant agreement 751859. J. L. acknowledges support from the Swiss National Science Foundation. N.G. is supported by the FRS-FNRS (Belgium) and the ERC Starting Grant TopoCold.

---

\* cecile.repellin@lpmmc.cnrs.fr

† ngoldman@ulb.ac.be

- [1] N. Goldman, J. C. Budich, and P. Zoller, “Topological quantum matter with ultracold gases in optical lattices,” *Nature Physics*, vol. 12, pp. 639–645, July 2016.
- [2] N. Cooper, J. Dalibard, and I. Spielman, “Topological bands for ultracold atoms,” *Reviews of Modern Physics*, vol. 91, no. 1, p. 015005, 2019.
- [3] J. Dalibard, F. Gerbier, G. Juzeliūnas, and P. Öhberg, “Colloquium: Artificial gauge potentials for neutral atoms,” *Reviews of Modern Physics*, vol. 83, pp. 1523–1543, Nov 2011.
- [4] N. Goldman, G. Juzeliūnas, P. Öhberg, and I. B. Spielman, “Light-induced gauge fields for ultracold atoms,” *Reports on Progress in Physics*, vol. 77, p. 126401, Dec. 2014.
- [5] M. Atala, M. Aidelsburger, J. T. Barreiro, D. Abanin, T. Kitagawa, E. Demler, and I. Bloch, “Direct measurement of the Zak phase in topological Bloch bands,” *Nature Physics*, vol. 9, no. 12, pp. 795–800, 2013.
- [6] M. Aidelsburger, M. Lohse, C. Schweizer, M. Atala, J. T. Barreiro, S. Nascimbène, N. R. Cooper, I. Bloch, and N. Goldman, “Measuring the Chern number of Hofstadter bands with ultracold bosonic atoms,” *Nature Physics*, vol. 11, pp. 162–166, Feb. 2015.
- [7] S. Nakajima, T. Tomita, S. Taie, T. Ichinose, H. Ozawa, L. Wang, M. Troyer, and Y. Takahashi, “Topological Thouless pumping of ultracold fermions,” *Nature Physics*, vol. 12, no. 4, pp. 296–300, 2016.
- [8] M. Lohse, C. Schweizer, O. Zilberberg, M. Aidelsburger, and I. Bloch, “A Thouless quantum pump with ultracold bosonic atoms in an optical superlattice,” *Nature Physics*, vol. 12, no. 4, pp. 350–354, 2016.
- [9] Z. Wu, L. Zhang, W. Sun, X.-T. Xu, B.-Z. Wang, S.-C. Ji, Y. Deng, S. Chen, X.-J. Liu, and J.-W. Pan, “Realization of two-dimensional spin-orbit coupling for Bose-Einstein condensates,” *Science*, vol. 354, no. 6308, pp. 83–88, 2016.
- [10] W. Sun, C.-R. Yi, B.-Z. Wang, W.-W. Zhang, B. C. Sanders, X.-T. Xu, Z.-Y. Wang, J. Schmiedmayer, Y. Deng, X.-J. Liu, *et al.*, “Uncover topology by quantum quench dynamics,” *Physical Review Letters*, vol. 121, no. 25, p. 250403, 2018.
- [11] N. Fläschner, D. Vogel, M. Tarnowski, B. S. Rem, D.-S. Lühmann, M. Heyl, J. C. Budich, L. Mathey, K. Sengstock, and C. Weitenberg, “Observation of a dynamical topological phase transition,” *Nature Physics*, vol. 14, pp. 265–268, 2018.
- [12] M. Tarnowski, F. N. Ünal, N. Fläschner, B. S. Rem, A. Eckardt, K. Sengstock, and C. Weitenberg, “Measuring topology from dynamics by obtaining the Chern number from a linking number,” *Nature Communications*, vol. 10, no. 1, pp. 1–13, 2019.
- [13] S. Sugawa, F. Salces-Carcoba, A. R. Perry, Y. Yue, and I. Spielman, “Second Chern number of a quantum-simulated non-Abelian Yang monopole,” *Science*, vol. 360, no. 6396, pp. 1429–1434, 2018.
- [14] M. Lohse, C. Schweizer, H. M. Price, O. Zilberberg, and I. Bloch, “Exploring 4D quantum Hall physics with a 2D topological charge pump,” *Nature*, vol. 553, no. 7686, pp. 55–58, 2018.
- [15] E. J. Meier, F. A. An, A. Dauphin, M. Maffei, P. Massignan, T. L. Hughes, and B. Gadway, “Observation of the topological Anderson insulator in disordered atomic wires,” *Science*, vol. 362, no. 6417, pp. 929–933, 2018.
- [16] S. de Léséleuc, V. Lienhard, P. Scholl, D. Barredo, S. Weber, N. Lang, H. P. Büchler, T. Lahaye, and A. Browaeys, “Observation of a symmetry-protected topological phase of interacting bosons with Rydberg atoms,” *Science*, vol. 365, no. 6455, pp. 775–780, 2019.
- [17] D. Genkina, L. M. Ayccock, H.-I. Lu, M. Lu, A. M. Pineiro, and I. Spielman, “Imaging topology of Hofstadter ribbons,” *New Journal of Physics*, vol. 21, no. 5, p. 053021, 2019.
- [18] L. Asteria, D. T. Tran, T. Ozawa, M. Tarnowski, B. S. Rem, N. Fläschner, K. Sengstock, N. Goldman, and C. Weitenberg, “Measuring quantized circular dichroism in ultracold topological matter,” *Nature physics*, vol. 15, no. 5, pp. 449–454, 2019.
- [19] B. S. Rem, N. Käming, M. Tarnowski, L. Asteria, N. Fläschner, C. Becker, K. Sengstock, and C. Weitenberg, “Identifying quantum phase transitions using artificial neural networks on experimental data,” *Nature Physics*, vol. 15, no. 9, pp. 917–920, 2019.
- [20] T. Chalopin, T. Satoor, A. Evrard, V. Makhalov, J. Dalibard, R. Lopes, and S. Nascimbene, “Exploring the topology of a quantum Hall system at the microscopic level,” *arXiv preprint arXiv:2001.01664*, 2020.
- [21] K. Wintersperger, C. Braun, F. N. Ünal, A. Eckardt, M. Di Liberto, N. Goldman, I. Bloch, and M. Aidelsburger, “Realization of anomalous Floquet topological phases with ultracold atoms,” *arXiv preprint arXiv:2002.09840*, 2020.
- [22] N. R. Cooper and J. Dalibard, “Reaching fractional quantum Hall states with optical flux lattices,” *Physical Review Letters*, vol. 110, no. 18, p. 185301, 2013.
- [23] N. Y. Yao, A. V. Gorshkov, C. R. Laumann, A. M. Läuchli, J. Ye, and M. D. Lukin, “Realizing fractional Chern insulators in dipolar spin systems,” *Physical Review Letters*, vol. 110, no. 18, p. 185302, 2013.
- [24] F. Grusdt, F. Letscher, M. Hafezi, and M. Fleischhauer, “Topological growing of Laughlin states in synthetic gauge fields,” *Physical Review Letters*, vol. 113, no. 15, p. 155301, 2014.
- [25] F. Grusdt and M. Hönig, “Realization of fractional Chern insulators in the thin-torus limit with ultracold bosons,” *Physical Review A*, vol. 90, no. 5, p. 053623, 2014.
- [26] Y.-C. He, F. Grusdt, A. Kaufman, M. Greiner, and A. Vishwanath, “Realizing and adiabatically preparing bosonic integer and fractional quantum Hall states in optical lattices,” *Physical Review B*, vol. 96, p. 201103, Nov 2017.
- [27] J. Motruk and F. Pollmann, “Phase transitions and adiabatic preparation of a fractional Chern insulator in a boson cold-atom model,” *Physical Review B*, vol. 96, p. 165107, Oct 2017.
- [28] C. Repellin, T. Yefsah, and A. Sterdyniak, “Creating a bosonic fractional quantum Hall state by pairing fermions,” *Physical Review B*, vol. 96, p. 161111, Oct 2017.

- [29] A. Hudomal, N. Regnault, and I. Vasić, “Bosonic fractional quantum Hall states in driven optical lattices,” *Physical Review A*, vol. 100, no. 5, p. 053624, 2019.
- [30] S. A. Parameswaran, R. Roy, and S. L. Sondhi, “Fractional quantum Hall physics in topological flat bands,” *Comptes Rendus Physique*, vol. 14, pp. 816–839, Nov. 2013.
- [31] E. J. Bergholtz and Z. Liu, “Topological flat band models and fractional Chern insulators,” *International Journal of Modern Physics B*, vol. 27, p. 1330017, Sept. 2013.
- [32] R. Palmer and D. Jaksch, “High-field fractional quantum Hall effect in optical lattices,” *Physical Review Letters*, vol. 96, no. 18, p. 180407, 2006.
- [33] J. A. Kjäll and J. E. Moore, “Edge excitations of bosonic fractional quantum Hall phases in optical lattices,” *Physical Review B*, vol. 85, no. 23, p. 235137, 2012.
- [34] W.-W. Luo, W.-C. Chen, Y.-F. Wang, and C.-D. Gong, “Edge excitations in fractional Chern insulators,” *Physical Review B*, vol. 88, no. 16, p. 161109, 2013.
- [35] F. Grusdt, N. Y. Yao, D. Abanin, M. Fleischhauer, and E. Demler, “Interferometric measurements of many-body topological invariants using mobile impurities,” *Nature Communications*, vol. 7, p. 11994, June 2016.
- [36] L. Taddia, E. Cornfeld, D. Rossini, L. Mazza, E. Sela, and R. Fazio, “Topological fractional pumping with alkaline-earth-like atoms in synthetic lattices,” *Physical Review Letters*, vol. 118, p. 230402, Jun 2017.
- [37] X.-Y. Dong, A. G. Grushin, J. Motruk, and F. Pollmann, “Charge excitation dynamics in bosonic fractional Chern insulators,” *Physical Review Letters*, vol. 121, no. 8, p. 086401, 2018.
- [38] M. Račiūnas, F. N. Únal, E. Anisimovas, and A. Eckardt, “Creating, probing, and manipulating fractionally charged excitations of fractional Chern insulators in optical lattices,” *Physical Review A*, vol. 98, p. 063621, Dec 2018.
- [39] R. Umucalılar, E. Macaluso, T. Comparin, and I. Carusotto, “Time-of-flight measurements as a possible method to observe anyonic statistics,” *Physical Review Letters*, vol. 120, no. 23, p. 230403, 2018.
- [40] C. Repellin and N. Goldman, “Detecting fractional Chern insulators through circular dichroism,” *Physical Review Letters*, vol. 122, no. 16, p. 166801, 2019.
- [41] T. Yoshida, K. Kudo, H. Katsura, and Y. Hatsugai, “Fate of fractional quantum Hall states in open quantum systems: characterization of correlated topological states for the full Liouvillian,” *arXiv preprint arXiv:2005.12635*, 2020.
- [42] Z.-P. Cian, H. Deghani, A. Elben, B. Vermersch, G. Zhu, M. Barkeshli, P. Zoller, and M. Hafezi, “Many-body Chern number from statistical correlations of randomized measurements,” *arXiv preprint arXiv:2005.13543*, 2020.
- [43] T. Ozawa, H. M. Price, A. Amo, N. Goldman, M. Hafezi, L. Lu, M. C. Rechtsman, D. Schuster, J. Simon, O. Zilberberg, and I. Carusotto, “Topological photonics,” *Reviews of Modern Physics*, vol. 91, no. 1, p. 015006, 2019.
- [44] P. Knüppel, S. Ravets, M. Kroner, S. Fält, W. Wegscheider, and A. Imamoglu, “Nonlinear optics in the fractional quantum Hall regime,” *Nature*, vol. 572, no. 7767, pp. 91–94, 2019.
- [45] L. W. Clark, N. Schine, C. Baum, N. Jia, and J. Simon, “Observation of Laughlin states made of light,” *arXiv preprint arXiv:1907.05872*, 2019.
- [46] S. M. Girvin, “The quantum Hall effect: novel excitations and broken symmetries,” in *Aspects topologiques de la physique en basse dimension. Topological aspects of low dimensional systems*, pp. 53–175, Springer, 1999.
- [47] J.-y. Choi, S. Kang, S. W. Seo, W. J. Kwon, and Y.-i. Shin, “Observation of a geometric Hall effect in a spinor Bose-Einstein condensate with a skyrmion spin texture,” *Physical Review Letters*, vol. 111, no. 24, p. 245301, 2013.
- [48] G. Jotzu, M. Messer, R. Desbuquois, M. Lebrat, T. Uehlinger, D. Greif, and T. Esslinger, “Experimental realization of the topological Haldane model with ultracold fermions,” *Nature (London)*, vol. 515, pp. 237–240, Nov. 2014.
- [49] R. Anderson, F. Wang, P. Xu, V. Venu, S. Trotzky, F. Chevy, and J. H. Thywissen, “Conductivity spectrum of ultracold atoms in an optical lattice,” *Physical Review Letters*, vol. 122, no. 15, p. 153602, 2019.
- [50] R. J. Fletcher, A. Shaffer, C. C. Wilson, P. B. Patel, Z. Yan, V. Crépel, B. Mukherjee, and M. W. Zwierlein, “Geometric squeezing into the lowest Landau level,” *arXiv preprint arXiv:1911.12347*, 2019.
- [51] L. J. LeBlanc, K. Jimenez-Garcia, R. A. Williams, M. C. Beeler, A. R. Perry, W. D. Phillips, and I. B. Spielman, “Observation of a superfluid Hall effect,” *Proceedings of the National Academy of Sciences*, vol. 109, no. 27, pp. 10811–10814, 2012.
- [52] D. R. Hofstadter, “Energy levels and wave functions of Bloch electrons in rational and irrational magnetic fields,” *Physical Review B*, vol. 14, no. 6, p. 2239, 1976.
- [53] A. S. Sorensen, E. Demler, and M. D. Lukin, “Fractional quantum Hall states of atoms in optical lattices,” *Physical Review Letters*, vol. 94, p. 086803, Mar 2005.
- [54] A. Dauphin and N. Goldman, “Extracting the Chern number from the dynamics of a fermi gas: Implementing a quantum Hall bar for cold atoms,” *Physical Review Letters*, vol. 111, no. 13, p. 135302, 2013.
- [55] A. Widom, “Thermodynamic derivation of the Hall effect current,” *Physica Letters A*, vol. 90, no. 9, p. 474, 1982.
- [56] P. Streda, “Theory of quantised Hall conductivity in two dimensions,” *Journal of Physics C: Solid State Physics*, vol. 15, no. 22, p. L717, 1982.
- [57] P. Streda and L. Smrcka, “Thermodynamic derivation of the Hall current and the thermopower in quantising magnetic field,” *Journal of Physics C: Solid State Physics*, vol. 16, no. 24, p. L895, 1983.
- [58] G. Giuliani and G. Vignale, *Quantum theory of the electron liquid*. Cambridge university press, 2005.
- [59] H. M. Price, O. Zilberberg, T. Ozawa, I. Carusotto, and N. Goldman, “Measurement of Chern numbers through center-of-mass responses,” *Physical Review B*, vol. 93, no. 24, p. 245113, 2016.
- [60] D. T. Tran, A. Dauphin, A. G. Grushin, P. Zoller, and N. Goldman, “Probing topology by “heating”: Quantized circular dichroism in ultracold atoms,” *Science Advances*, vol. 3, p. e1701207, Aug. 2017.
- [61] W. Kohn, “Cyclotron resonance and de Haas-van Alphen oscillations of an interacting electron gas,” *Physical Review*, vol. 123, no. 4, p. 1242, 1961.
- [62] C. Mudry, *Lecture notes on field theory in condensed matter physics*. World Scientific Publishing Company, 2014.
- [63] The COM dynamics remains classical upon adding a harmonic trap [58, 61].
- [64] Q. Niu, D. J. Thouless, and Y.-S. Wu, “Quantized Hall conductance as a topological invariant,” *Physical Review B*, vol. 31, pp. 3372–3377, Mar 1985.
- [65] R. Tao and F. Haldane, “Impurity effect, degeneracy, and topological invariant in the quantum Hall effect,” *Physical Review B*, vol. 33, no. 6, p. 3844, 1986.
- [66] I. Bloch, J. Dalibard, and W. Zwerger, “Many-body physics with ultracold gases,” *Reviews of Modern Physics*, vol. 80,

- no. 3, p. 885, 2008.
- [67] M. E. Tai, A. Lukin, M. Rispoli, R. Schittko, T. Menke, Dan Borgnia, P. M. Preiss, F. Grusdt, A. M. Kaufman, and M. Greiner, “Microscopy of the interacting Harper-Hofstadter model in the two-body limit,” *Nature (London)*, vol. 546, pp. 519–523, June 2017.
- [68] M. Hafezi, A. S. Sørensen, E. Demler, and M. D. Lukin, “Fractional quantum Hall effect in optical lattices,” *Physical Review A*, vol. 76, p. 023613, Aug 2007.
- [69] We refer to the infinite plane geometry, where the FQH droplet is confined through total angular momentum conservation, not by a confinement potential.
- [70] *see Supplementary Material.*
- [71] The  $\nu = 2/3$  Jain fraction is a possible candidate among these phases [33, 82], but we did not identify any unambiguous signature of this phase in our setting.
- [72] In the continuum, a hard confinement was shown to have a drastic influence on the energy of edge modes [83, 84].
- [73] A. Sterdyniak, N. Regnault, and B. A. Bernevig, “Extracting excitations from model state entanglement,” *Physical Review Letters*, vol. 106, p. 100405, Mar 2011.
- [74] F. D. M. Haldane, ““Fractional statistics” in arbitrary dimensions: A generalization of the Pauli principle,” *Physical Review Letters*, vol. 67, pp. 937–940, Aug 1991.
- [75] D. J. Thouless, M. Kohmoto, M. P. Nightingale, and M. den Nijs, “Quantized Hall conductance in a two-dimensional periodic potential,” *Physical Review Letters*, vol. 49, no. 6, p. 405, 1982.
- [76] M. Kohmoto, “Zero modes and the quantized Hall conductance of the two-dimensional lattice in a magnetic field,” *Physical Review B*, vol. 39, no. 16, p. 11943, 1989.
- [77] R. Bianco and R. Resta, “Mapping topological order in coordinate space,” *Physical Review B*, vol. 84, no. 24, p. 241106, 2011.
- [78] D.-T. Tran, A. Dauphin, N. Goldman, and P. Gaspard, “Topological Hofstadter insulators in a two-dimensional quasicrystal,” *Physical Review B*, vol. 91, no. 8, p. 085125, 2015.
- [79] N. H. Lindner, A. Auerbach, and D. P. Arovas, “Vortex quantum dynamics of two dimensional lattice bosons,” *Physical Review Letters*, vol. 102, no. 7, p. 070403, 2009.
- [80] J. Motruk and I. Na, “Detecting fractional Chern insulators in optical lattices through quantized displacement,” *arXiv:2005.09860*, 2020.
- [81] J. Hauschild and F. Pollmann, “Efficient numerical simulations with Tensor Networks: Tensor Network Python (TeNPy),” *SciPost Physics Lecture Notes*, vol. 5, 2018, code available from <https://github.com/tenpy/tenpy>, *arXiv:1805.00055*, 2018.
- [82] G. Möller and N. R. Cooper, “Composite fermion theory for bosonic quantum Hall states on lattices,” *Physical Review Letters*, vol. 103, p. 105303, Sep 2009.
- [83] R. Fern and S. H. Simon, “Quantum Hall edges with hard confinement: Exact solution beyond Luttinger liquid,” *Physical Review B*, vol. 95, p. 201108, May 2017.
- [84] E. Macaluso and I. Carusotto, “Hard-wall confinement of a fractional quantum Hall liquid,” *Physical Review A*, vol. 96, p. 043607, Oct 2017.
- [85] R. O. Umucalilar, H. Zhai, and M. Ö. Oktel, “Trapped Fermi Gases in Rotating Optical Lattices: Realization and Detection of the Topological Hofstadter Insulator,” *Physical Review Letters*, vol. 100, p. 070402, Feb 2008.
- [86] T. Fukui and T. Fujiwara, “Streda formula for the Hofstadter-Wilson-Dirac model in two and four dimensions,” *Journal of the Physical Society of Japan*, vol. 85, p. 124709, Nov 2016.
- [87] M. P. Zaletel, R. S. K. Mong, C. Karrasch, J. E. Moore, and F. Pollmann, “Time-evolving a matrix product state with long-ranged interactions,” *Physical Review B*, vol. 91, no. 16, p. 165112, 2015.
- [88] S. Powell, R. Barnett, R. Sensarma, and S. D. Sarma, “Bogoliubov theory of interacting bosons on a lattice in a synthetic magnetic field,” *Physical Review A*, vol. 83, no. 1, p. 013612, 2011.
- [89] T. Ozawa, H. M. Price, and I. Carusotto, “Momentum-space Harper-Hofstadter model,” *Physical Review A*, vol. 92, no. 2, p. 023609, 2015.

## Supplementary material for: “Hall drift of fractional Chern insulators in few-boson systems”

### Appendix A: Ground state properties and Hall drifts

- (a) Stability of the Hall plateau and bulk density evaluation
- (b) Hall drift in larger systems: DMRG results
- (c) Extracting  $\sigma_H$  from the particle density: Streda’s formula
- (d) Minimal configurations: 3 and 4 bosons

### Appendix B: Methods

- (a) Ramps used in numerical calculations
- (b) Particle entanglement spectrum
- (c) Exact diagonalization: ground state and time-evolution calculations
- (d) DMRG: ground state and time-evolution calculations
- (e) The case of non-interacting fermions

### Appendix C: Single-particle Hofstadter spectrum in a small circular box

#### APPENDIX A: GROUND-STATE PROPERTIES AND HALL DRIFTS

In the main text, we have shown numerical data for  $N = 4$  hardcore bosons prepared in a circular box of  $N_s = 60$  sites. We have obtained consistent results for other particle numbers  $N$  and lattice sizes  $N_s$ , (corresponding to other densities  $\rho$ ), which we present in this Appendix.

##### (a) Stability of the Hall plateau and bulk density evaluation

Extracting the Hall conductivity  $\sigma_H$  from the center-of-mass (COM) Hall drift requires the evaluation of the bulk density  $\rho_{\text{bulk}}$ , according to the formula [see main text]

$$\sigma_H/\sigma_0 = (2\pi\rho_{\text{bulk}}/F)v_{\perp}. \quad (2)$$

For large enough systems, one can evaluate  $\rho_{\text{bulk}}$  by taking the average of the density over a central circular region, whose radius is large compared to the lattice spacing but small compared to the radius of the atomic cloud. In few-boson systems, which are the focus of this work, such scale separation may not exist. In particular, in the configuration studied in the main text ( $N = 4$  bosons initially confined in  $N_s = 60$  sites), one notices substantial spatial fluctuations of the particle density.

Here, we analyze the impact of such density fluctuations on the extracted Hall conductivity [Fig. (4) in the main text]. To do so, we evaluate  $\rho_{\text{bulk}}$  as the average particle density within a small and central circular region of radius  $r_{\text{bulk}}$ , considering values in the range  $r_{\text{bulk}} \in [0.4r_0, 0.6r_0]$ , where  $r_0$  is the radius of the (initial) circular box containing  $N_s$  sites. We illustrate the impact of this radius choice in Figure 5, which shows  $\sigma_H$  as extracted from the COM Hall drift [Eq. (2)] for three different choices. Interestingly, the Hall plateau

displayed in the main text [Fig. (4)] is very robust: neither its existence, nor its position and range on the flux axis, depend on the radius  $r_{\text{bulk}}$  used to evaluate the bulk density. While the exact value of  $\sigma_H/\sigma_0$  depends on  $r_{\text{bulk}}$ , one notices that  $\sigma_H/\sigma_0 \approx 0.5$  on this plateau for all choices.

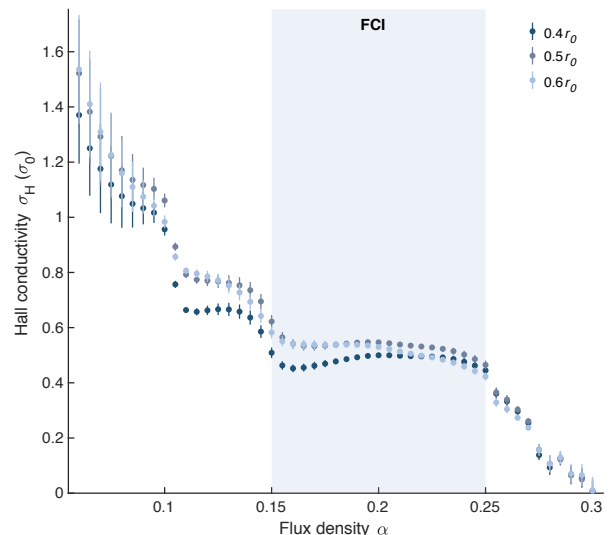


Figure 5. Impact of the bulk density evaluation on the determination of  $\sigma_H$  for a few-boson system. The configuration is the same as in the main text (Fig. 4):  $N = 4$  hardcore bosons initially confined in a circular box of  $N_s = 60$  sites, in the HHH model. Here, we determined  $\rho_{\text{bulk}}$  as the average particle density within a central circular region of radius  $r_{\text{bulk}}$ , with  $r_{\text{bulk}} = 0.4r_0$ ,  $r_{\text{bulk}} = 0.5r_0$  and  $r_{\text{bulk}} = 0.6r_0$ , where  $r_0$  is the radius of the initial circular box ( $N_s = 60$ ); these three radii correspond respectively to 12, 16 and 24 sites. In this small system, the radius choice affects the value of  $\sigma_H$ , as extracted from the COM Hall drift [Eq. (2)]; however, the existence of the Hall plateau, as well as its position and range along the flux axis, are robust.

### (b) Hall drift in larger systems: DMRG results

We used DMRG to extend our results to larger system sizes (with  $N = 5$  to  $N = 10$  bosons); methodological details of the DMRG simulations are given in Appendix B. We simulated the Hall drift of up to  $N = 10$  hardcore bosons, initially prepared in a circular box of  $N_s = 120$  sites and released into a square box of 256 sites; see Fig. 6. The particle density in the ground state [Fig. 6(a)] depicts a plateau in the central region; as a result, the value of  $\rho_{\text{bulk}}$  is relatively insensitive to the radius  $r_{\text{bulk}}$  chosen for its evaluation. In order to extract  $\sigma_H$  from the COM Hall drift [Eq. (2)], we evaluated  $\rho_{\text{bulk}}$  as the average density in a circle of 16 sites; the results are shown in Fig. 6(c). As expected for a  $\nu = 1/2$  FCI phase, the value of the Hall conductivity on the plateau approaches the many-body Chern number  $\sigma_H/\sigma_0 = 0.5$ . We point out that the approached quantization is already accurate up to  $\simeq 5\%$  for this system of  $N = 10$  bosons.

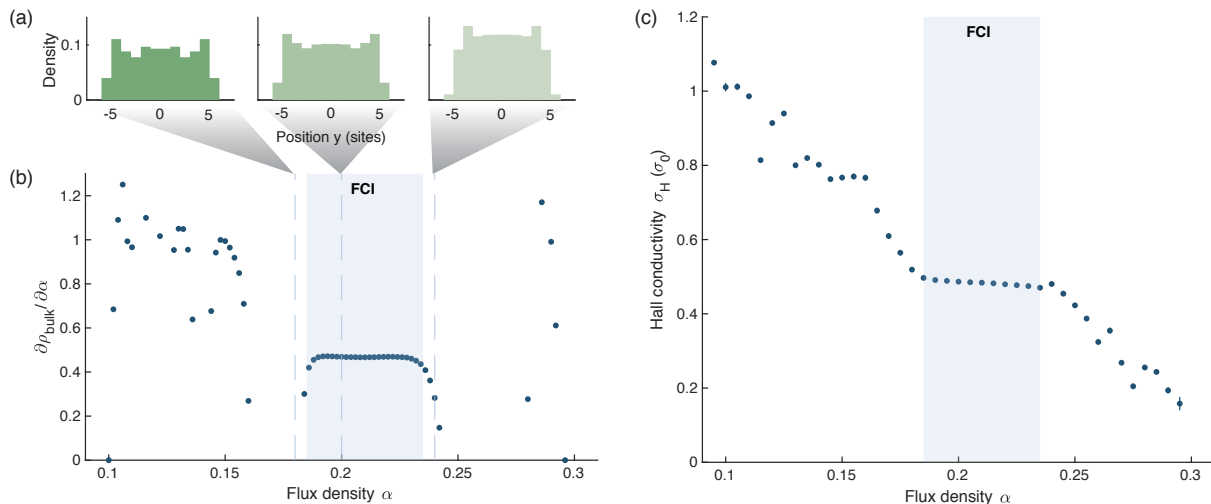


Figure 6. Properties of a system of  $N = 10$  hardcore bosons in a circular box of  $N_s = 120$  sites in the Harper-Hofstadter-Hubbard model, obtained using DMRG. The left column shows the characterization of the ground state through static signatures: (a) Particle density; (b) Derivative of the bulk particle density  $\rho_{\text{bulk}}$  with respect to the flux density [in the FCI phase, it satisfies Streda’s formula in Eq. (3)]. (c) Hall conductivity as extracted from the COM Hall drift upon releasing the ground state into a square with 256 sites and applying a force  $F = 0.04J/d$ . The bulk density  $\rho_{\text{bulk}}$  was evaluated as the average density in a circle comprising 16 sites.

### (c) Extracting $\sigma_H$ from the particle density: Streda’s formula

For an incompressible phase, the variation of the bulk density  $\rho_{\text{bulk}}$  with respect to the flux density  $\alpha$  is directly related to the quantized Hall conductivity. This relation, which is known as Streda’s formula [55–59, 85, 86], reads in our units

$$\sigma_H/\sigma_0 = \frac{\partial \rho_{\text{bulk}}}{\partial \alpha}. \quad (3)$$

Applying this approach to the  $\nu = 1/2$  FCI phase, one thus expects the existence of a plateau  $\partial \rho_{\text{bulk}}/\partial \alpha \approx 0.5$  within the corresponding flux range. We have validated this prediction for  $N = 10$  hardcore bosons in  $N_s = 120$  sites; see Fig. 6(b).

While we still observe a smooth variation of  $\partial \rho_{\text{bulk}}/\partial \alpha$  within the FCI phase of smaller systems, large density fluctuations complicate a direct application of Streda’s formula in those configurations.

### (d) Minimal configurations: 3 and 4 bosons

We sought for minimal configurations that exhibit Hall-plateau signatures of the FCI state, by simulating the Hall drift protocol for various system sizes  $N_s$  and number of bosons  $N$ . For both  $N = 3$  and  $N = 4$ , we hereby show the exact-diagonalization results obtained for the smallest system size where Hall-drift signatures of a  $\nu = 1/2$  FCI state were found:  $N_s = 40$  for  $N = 3$  and  $N_s = 49$  for  $N = 4$ .

Figure 7 shows the ground-state properties and the center-of-mass Hall drift for  $N = 4$  bosons and  $N_s = 49$  sites. Based on the low-energy spectra and entanglement spectroscopy, we find clear signatures of the  $\nu = 1/2$  FCI state for  $0.18 \leq \alpha \leq 0.29$ . We point out that this shift of the FCI phase towards larger values of  $\alpha$  compared to the case presented in the main text ( $N = 4$ ,  $N_s = 60$ , where the FCI regime corresponds to  $0.15 \leq \alpha \leq 0.25$ ; see Fig. 2 in the main text) is consistent with a larger particle density  $\rho = N/N_s$ .

We observe an emergent Hall plateau for  $\alpha \geq 0.18$ . We note that its width is slightly smaller than the FCI region; as shown in the main text (using  $N_s = 60$  sites for  $N = 4$  bosons), this discrepancy is reduced by increasing the system size, which suggests that it is due to the smallness of this minimal setting ( $N_s = 49$  sites for  $N = 4$  bosons). We note that additional plateau features appear for each gap opening in the finite-size energy spectrum.

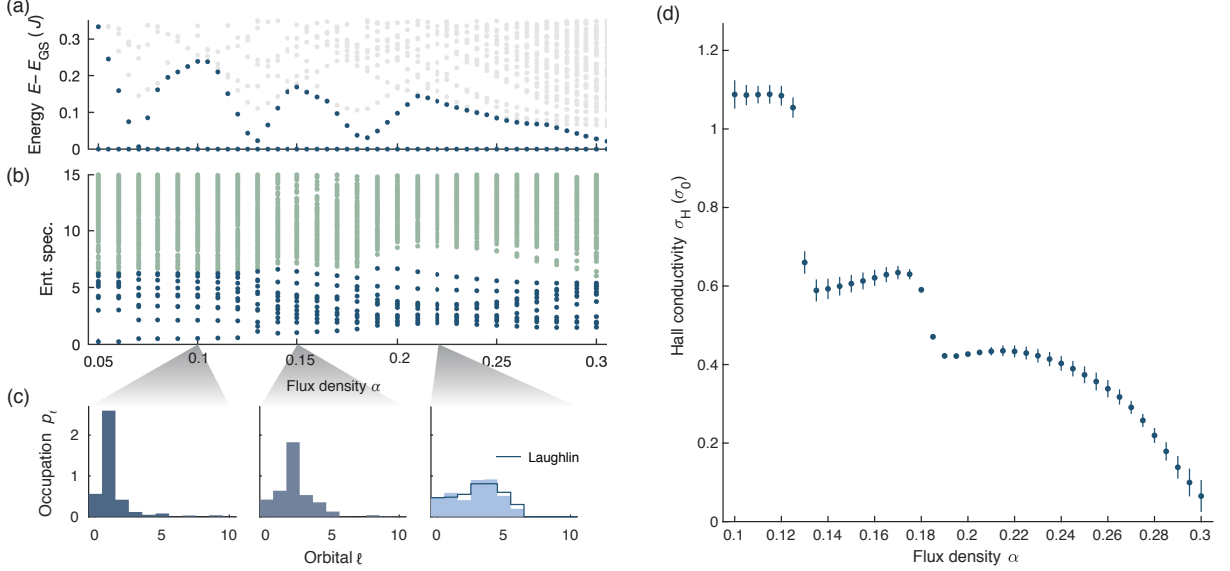


Figure 7. Properties of a system of  $N = 4$  hardcore bosons in a circular box of  $N_s = 49$  sites in the Harper-Hofstadter-Hubbard model. The left column shows the characterization of the ground state through static signatures (following Fig. 2 of the main text): (a) Energy spectrum; (b) Particle Entanglement Spectrum; (c) Occupation of the single-particle orbitals in the ground state, in increasing energy order (the line shows the orbital occupation for the  $N = 4$  Laughlin state on the disk, where the orbitals are sorted in increasing angular momentum); (d) Hall conductivity as extracted from the COM Hall drift upon releasing the ground state into a circle with 113 sites and applying a force  $F = 0.0001J/d$ . The bulk density  $\rho_{\text{bulk}}$  was evaluated as the average particle density within a circle comprising 9 sites ( $r_{\text{bulk}} = 0.5r_0$ ).

For  $N = 3$  bosons, the particle entanglement spectrum (PES) cannot provide a topological signature of the FCI. Indeed the PES that results from the only available particle bipartition ( $2 + 1$ ) corresponds to the spectrum of the single-particle density matrix (which cannot probe topological order). Nevertheless, for  $N = 3$  bosons and  $N_s = 40$  sites, the low-energy many-body spectrum and the orbital occupation are compatible with a FCI state in the flux window  $0.16 \leq \alpha \leq 0.28$ , where the Hall drift simulation reveals an emergent Hall plateau; see Fig. 8.

## APPENDIX B: METHODS

### (a) Ramps used in numerical calculations

In the Hall-drift protocol described in the main text, the force  $F(t)$  and the tunneling terms  $J(r, t)$  are slowly ramped up until reaching a stationary regime at  $t = \tau_{\text{ramp}}$ ; here  $r$  denotes the radial coordinate on the 2D plane. In our numerical calculations, the force is ramped up according to the first-order smoothstep function

$$F(t) = F \left( 3 \left( \frac{t}{\tau_{\text{ramp}}} \right)^2 - 2 \left( \frac{t}{\tau_{\text{ramp}}} \right)^3 \right), \quad (4)$$

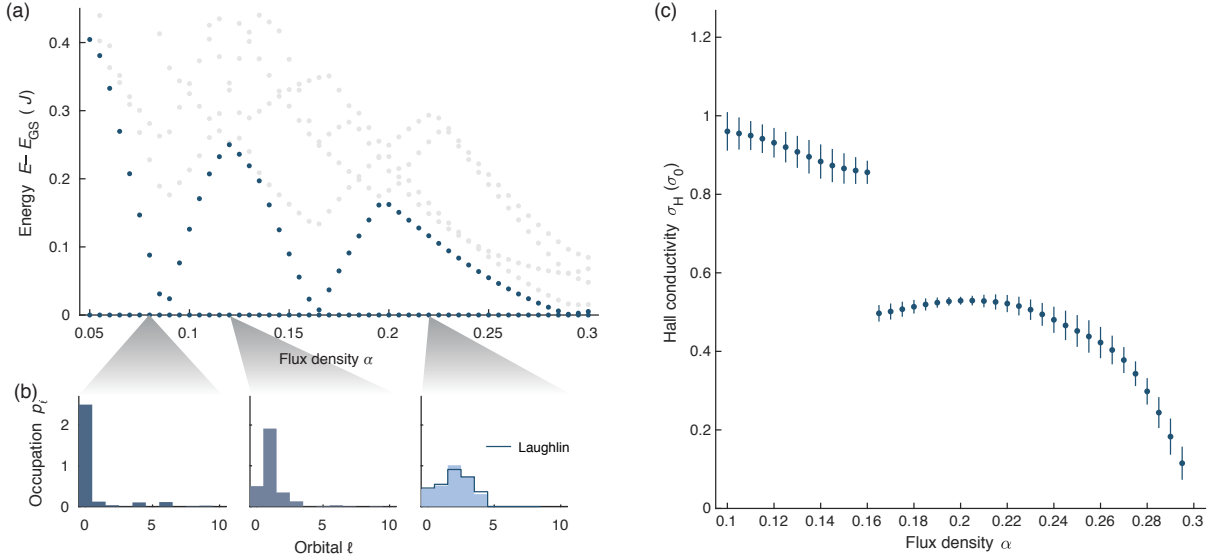


Figure 8. Properties of a system of  $N = 3$  hardcore bosons in an elliptic box of  $N_s = 40$  sites in the Harper-Hofstadter-Hubbard model. The left column shows the characterization of the ground state through static signatures: (a) Energy spectrum; (b) Occupation of the single-particle orbitals in the ground state, in increasing energy order (the line shows the orbital occupation for the  $N = 3$  Laughlin state on the disk, where the orbitals are sorted in increasing angular momentum); (c) Hall conductivity as extracted from the COM Hall drift upon releasing the ground state into an ellipse with 100 sites and applying a force  $F = 0.0001J/d$ . The bulk density  $\rho_{\text{bulk}}$  was evaluated as the average particle density within a circle comprising 8 sites ( $r_{\text{bulk}} = 0.5r_0$ ).

while we have used an exponential ramp for the tunneling terms,

$$J(r, t) = J \exp\left(-\frac{r - r_0}{r_1} \left(\frac{\tau_{\text{ramp}}}{t} - 1\right)\right), \quad (5)$$

where  $r_0$  is the radius of the small circular box where the initial state is prepared, and  $r_1$  is the radius of the larger circular box (i.e. the simulation box) into which it is released. These ramps were used both for the hardcore-boson (exact diagonalization and DMRG) and non-interacting-fermion cases. We expect that the exact form of the ramps should not be crucial in view of reaching a stationary regime, as long as they are smooth enough. Besides, we have verified that the linear-response regime is reached when using a weak force  $F \lesssim 0.04J/d$ .

### (b) Particle entanglement spectrum

We obtain the ground state  $|\Psi_{\text{GS}}\rangle$  of the HHH model using exact diagonalization. Here, we consider  $N = 4$  hardcore bosons in a box of  $N_s = 60$  sites. We consider a bipartition of the system with  $N_A = 2$  (resp.  $N_B = N - N_A = 2$ ) bosons in  $N_s$  sites in subsystem  $A$  (resp.  $B$ ). The particle entanglement spectrum [73] (PES) is the spectrum of  $-\log \hat{\rho}_A$ , where  $\hat{\rho}_A = \text{Tr}_B \hat{\rho}$  is the reduced density matrix obtained by tracing  $\hat{\rho} = |\Psi_{\text{GS}}\rangle\langle\Psi_{\text{GS}}|$  over the subsystem  $B$ .

### (c) Exact diagonalization: ground state and time-evolution calculations

For systems with  $N \leq 4$  hardcore bosons, our numerical results were obtained using exact diagonalization. To obtain the initial state, we first calculate the ground state  $|\Psi_{\text{GS}}\rangle$  of the HHH model in a small circular box of  $N_s$  sites. This state is then embedded in a larger circular box, by performing the direct product of  $|\Psi_{\text{GS}}\rangle$  with several empty sites. The state  $|\Psi(t + \delta_t)\rangle$  at time  $t + \delta_t$  is obtained by applying the unitary time-evolution operator  $\hat{U}(t) = e^{-i\hat{H}(t)\delta_t}$  onto  $|\Psi(t)\rangle$  for a small time interval  $\delta_t = 0.05J^{-1}$ ; here  $\hat{H}(t)$  is the Hamiltonian acting on  $N$  bosons in the large circular box; it corresponds to the HHH Hamiltonian in Eq. (1) with uniform tunneling amplitude  $J$  in the inner circular region, and tunneling amplitude  $J(r, t)$  in the outer region; it also contains the potential gradient realizing the uniform force  $F(t)$ . During the ramp,  $0 \leq t < \tau_{\text{ramp}} = 8J^{-1}$ , the time-dependent quantities  $F(t)$  and  $J(r, t)$  are given by Eqs (4)-(5). After the ramp,  $F(t) = F$  is constant and the tunneling

amplitude is constant and uniform throughout the entire system. The time-evolution operator  $\hat{U}(t)$  is evaluated using a series expansion with accuracy  $10^{-15}$ .

#### (d) DMRG: ground state and time-evolution calculations

For systems with more than  $N=4$  particles, where exact diagonalization becomes prohibitively costly, we have used DMRG. We first calculate the ground state  $|\Psi_{\text{GS}}\rangle$  of the HHH model in a small circular box of  $N_s$ . This box is embedded from the start in a larger rectangular box, but the bosons are initially confined to the small box due to the absence of tunneling terms to the outer sites. The size of the rectangular box is chosen to be large enough to permit a stationary regime during the Hall drift protocol. For the Hall drift protocol, we performed the time-evolution using the matrix product operator algorithm introduced in Ref. 87 with the WII expression for the time-evolution operator, and a time step  $\delta_t = 0.02J^{-1}$ . We verified that the error due to this finite time step was smaller than the linear fit error associated with the extraction of the Hall velocity  $v_{\perp}$ . For  $N = 10$  and  $N_s = 120$ , the results shown here were obtained with a bond dimension  $\chi = 500$ ; we have verified that using  $\chi = 800$  only resulted in a negligible difference of the COM motion.

#### (e) The case of non-interacting fermions

We first calculate the ground state of  $N$  fermions in the non-interacting Harper-Hofstadter model, within a circular box containing  $N_s$  sites. This sets our initial state  $|\Psi_{\text{GS}}\rangle$ , for a given flux density  $\alpha$ . In our calculations, we set  $N \approx N_s/4$  so that the particle density is close to quarter filling  $\rho \approx 1/4$ . We then obtain the time evolution operator  $\hat{U}_{\text{ramp}}$  describing the ramp, during which both the force and the tunneling into the larger lattice are activated; since the corresponding Hamiltonian is explicitly time-dependent, we discretize the time evolution in small time steps  $\Delta_t = 0.1J^{-1}$ ; the full duration of the ramp is  $\tau_{\text{ramp}} = 15J^{-1}$ . From this, we calculate the state at the end of the ramp through  $|\Psi_{\text{ramp}}\rangle = \hat{U}_{\text{ramp}}|\Psi_{\text{GS}}\rangle$ . Finally, the center-of-mass of the system is monitored by calculating the time-evolution of the state after the ramp,  $|\Psi(t)\rangle = \hat{U}_{\text{hold}}(t)|\Psi_{\text{ramp}}\rangle$ , in the presence of the constant force.

The local (real-space) Chern number  $\nu_{\text{Ch}}^{\text{local}} = 0.91$  indicated in Fig. 3 is calculated using the formulas of Refs. [77, 78] for  $N = 20$  fermions in a circular box of  $N_s = 81$  sites, and a flux density  $\alpha = 0.25$ . It is obtained by averaging the local Chern marker over 29 sites, located in a circular region at the center of the bulk.

### APPENDIX C: SINGLE-PARTICLE HOFSTADTER SPECTRUM IN A SMALL CIRCULAR BOX

We show the single-particle Hofstadter spectrum for a lattice of  $N_s = 60$  sites in Fig. 9, for three representative values of the flux  $\alpha$ . To label the eigenstates, we use the eigenvalues of the  $C_4$ -rotation operator; in this system with discrete rotational symmetry [88, 89], they are equivalent to the angular momentum modulo 4.

Considering this lattice of  $N_s = 60$  sites and a flux  $\alpha \approx 0.2$ , we have shown that the ground state of  $N = 4$  hardcore bosons can be identified as a  $\nu = 1/2$  FCI ground state (see main text). In this setting, only the 7 lowest-energy orbitals have a substantial occupation in this ground state [see Fig.2(c) of the main text]. In Fig. 9, we show that these 7 orbitals form the nearly-flat lowest band of the single-particle spectrum at  $\alpha = 0.2$ .

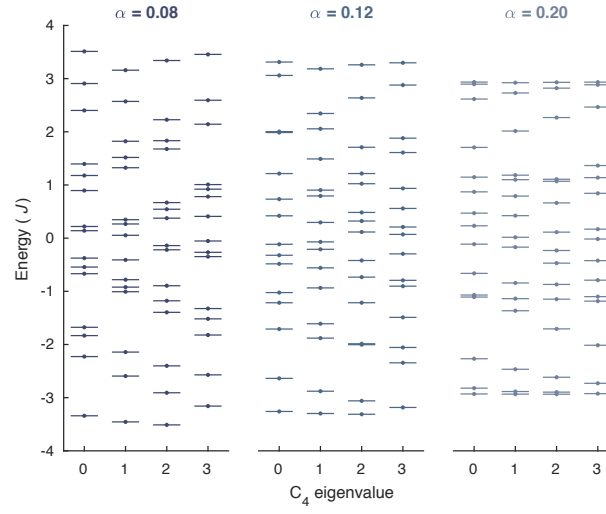


Figure 9. Single-particle spectrum for  $N_s = 60$  sites and flux density  $\alpha = 0.08, 0.12$  and  $0.2$ , labeled according to the eigenvalues of the  $C_4$ -rotation operator. The occupation of each of these orbitals in the  $N=4$  hardcore-boson configuration is given in Fig. 2(c) of the main text.